The role of metal nanoparticles in the catalytic production of single-walled carbon nanotubes—a review

The role of metal nanoparticles in the catalytic production of single-walled carbon nanotubes—a review

Anna Moisala[1]**, Albert G Nasibulin**[1] **and Esko I Kauppinen**[1,2]

[1] Centre for New Materials, Helsinki University of Technology, PO Box 1602, 02044 VTT, Finland
[2] Aerosol Technology Group, VTT Processes, PO Box 1602, 02044 VTT, Finland

E-mail: Esko.Kauppinen@vtt.fi

Abstract

Recent progress in chemical vapour deposition and aerosol synthesis of single-walled carbon nanotubes (SWCNTs) is reviewed with an emphasis on the role of metal nanoparticles in the processes. The effect of the various parameters on SWCNT formation is reported on the basis of published experiments. Evolution of the catalyst particle size distribution due to collision, sintering and evaporation of metal during SWCNT synthesis is discussed. The active catalyst has been demonstrated to be in a reduced metal form by comparison of the experimental data and calculations regarding the equilibrium concentration of carbon and oxygen in iron. Also the effect of the catalyst particle size on melting temperature and carbon solubility in metal is discussed. The stability of different carbon precursors (hydrocarbons and carbon monoxide) is considered thermodynamically. Furthermore, estimation of the maximum length of 1 and 2.5 nm diameter SWCNTs as a function of carbon solubility is conducted to determine whether carbon dissolution and precipitation are simultaneous or subsequent process steps.

(Some figures in this article are in colour only in the electronic version)

1. Introduction

Since their discovery several different production methods have been introduced to synthesize carbon nanotubes (CNTs). These methods can be broadly divided into chemical and physical according to the method applied to release carbon atoms from carbon-containing precursor molecules. In the physical methods (e.g. arc discharge [1] and laser ablation [2]) high-energy input is used to release the carbon atoms. The chemical methods rely on carbon atomization via catalytic decomposition of carbon precursors on the surface of transition metal particles.

The chemical methods can be further divided into chemical vapour deposition (CVD) [3] and aerosol synthesis (e.g. [4]) of CNTs. In CVD methods, the decomposition of the carbon precursor and CNT formation take place on the surface of previously made catalyst particles that are supported on a surface. In aerosol synthesis the catalyst particles are formed *in situ* during the CNT synthesis and the whole process takes place in the gas phase. The terms 'gas-phase synthesis' and 'floating catalyst method' have been applied in the literature for processes taking place either entirely or partly in the gas phase. We use the term 'aerosol synthesis' to specify processes taking place completely in the gas phase.

The growth mechanisms of CNTs remain somewhat controversial despite all the efforts made to both experimentally and theoretically validate competing theories. However, a few basic steps are generally acknowledged in the chemical CNT production regardless of whether the growth takes place in the gas phase or on a support surface (e.g. [3]). The catalytic decomposition of the carbon precursor molecules on the surface of the metal catalyst particles is followed by diffusion of the released carbon atoms into the metal particles. Carbon saturation in the metal occurs either by reaching the carbon solubility limit in the metal at a given temperature or by lowering the solubility limit via a temperature decrease. Supersaturation results in solid carbon precipitation from the metal particles. The physical form of the precipitated carbon depends on several parameters, including catalyst particle size (e.g. [5]) and precipitation rate [6] as described in more detail in the following sections.

The formation of several different carbonaceous products, including multiwalled carbon nanotubes (MWCNTs), single-walled carbon nanotubes (SWCNTs), amorphous carbon and metal particles encapsulated by graphitic shells, is possible during chemical CNT synthesis. Recently several groups have reported progress toward selective production of SWCNTs via chemical methods as reviewed in the following sections.

In this paper we review the development in production of SWCNTs via CVD and aerosol synthesis methods and discuss the mechanisms of carbon precursor decomposition and SWCNT nucleation and growth with an emphasis on the role of the catalyst metal particles in the synthesis. The physical methods for SWCNT formation or the processes combining physical and chemical methods (e.g. plasma enhanced CVD) are not covered here. Also the production of carbonaceous products other than SWCNTs is outside the scope of this review. Furthermore, we do not attempt to discuss the applications or properties of the SWCNTs. For that information we recommend the reader to refer to Dai [7] and to Dresselhaus *et al* [8].

2. Chemical vapour deposition

During CVD synthesis, previously made supported catalyst material is placed in a furnace. After the furnace is heated to the appropriate reaction temperature, a flow of gaseous carbon precursor is introduced for a given time period. Heating periods can reach several hours. The reaction product is collected from the reactor walls and support surfaces after cooling. Several different experimental conditions have been applied in CVD production of SWCNTs as summarized in table 1. Catalyst and carbon precursors, flow rates, reaction temperatures and batch run-times together with support materials are presented when available. Also the SWCNT product properties and the size of the catalyst particles before the SWCNT growth are listed as presented by the authors.

The growth mechanisms in the CVD process have been generally divided into two distinct methods: root and tip growth (e.g. [9]). In root growth, the catalyst particle stays pinned at the support surface and the support–particle interaction must be taken into consideration. On the contrary, the tip-growth mechanism takes place when the catalyst is lifted off from the support surface during CNT growth due to weak support–catalyst interaction. Experimental evidence

Table 1. Experimental conditions and product properties in CVD. NA = data not available, D = SWCNT diameter, L = SWCNT length, D_{ave} = average diameter, D_B = bundle diameter, L_B = bundle length, D_P = catalyst particle diameter, D_{CNT} = CNT diameter, number of walls not specified.

Catalyst particle size (nm)[a]	Catalyst precursor compound[b]	Carbon precursor, flow rate ($cm^3\ min^{-1}$)	Additive, flow rate ($cm^3\ min^{-1}$)	Reaction temperature (°C)	Reaction time (min)	Support material	Properties of individual SWCNTs (if not otherwise specified)[d]	References
NA	$Fe_2(SO_4)_3$, $Fe(NO_3)_3$, $(NH_4)_6Mo_7O_{24}$, $Ru(acac)_3$	CH_4, 6000		900	2–45	Al_2O_3 (powder), SiO_2 (sol–gel), Al_2O_3–SiO_2	Individual and tab bundles D = 0.7–5 nm (few DWCNTs)	[9]
NA	$Mo(acac)_2$, $Fe(NO_3)_3$	CO, 1200 C_2H_4, 0.66		700–850	<1200	Al_2O_3 (powder)	Individual and bundles D_{CNT} = 0.5–3 nm (few DWCNTs)	[22]
1–3	$(NH_4)Fe(SO_4)_2$	CH_4, 1000		900	5	Al_2O_3 (membrane on gold TEM grid)	Individual $D \sim D_P \sim$ 1–3 nm, L = 2 –420 nm	[14]
NA	$Fe(NO_3)_3$, $Ni(NO_3)_2$, $Co(NO_3)_2$	CH_4, 6150		1000	10	Al_2O_3 (powder), SiO_2 (powder)	Individual and bundles D = 1.3–5.4 nm, L_{SWCNT} < 10 μm, D_B = 4–47 nm, L_B < tens of μm	[25]
1–2, 3–5	$(NH_4)Fe(SO_4)_2$	CH_4, 200	H_2, 200	900	5	SiO_2 (oxidized Si) Al_2O_3 (membrane on gold TEM grid)	Individual and bundles, D = 3.0 ± 0.9 nm, 1.5 ± 0.4 nm, L = few nm to 20 μm (AFM)	[13]
NA	$Fe_2(SO_4)_3$, $MoO_2(acac)_2$	CH_4, 1000		850–1000	<400	Al_2O_3 (aerogel)	Bundles D = 0.9–2.7 nm, D_B = 10–20 nm	[26]
NA 1–2	$(NH_4)Fe(SO_4)_2$, $FeCl_3$	CH_4, 1000+ C_2H_4, 20	H_2, 500	900	10	SiO_2 (oxidized Si)	D = 1–3 nm, L = 1–600 μm	[15, 16, 18]
NA	$MoO_2(acac)_2$	CO, 1200		1200	60	Al_2O_3 (powder)	Individual $D \sim$ 1–5 nm, $L \sim$ 100 nm to several μm	[3]
NA	$Fe(NO_3)_3$, $Fe_2(SO_4)_3$, $(NH_4)_6Mo_7O_{24}$	CH_4, 40	Ar, 350	680–900	60	Al_2O_3 (powder)	Bundles $D_{B,ave} \sim$ 10 nm, individual $D_{ave} \sim$ 1.5 nm	[20]

Table 1. (Continued.)

Catalyst particle size (nm)^a	Catalyst precursor compound^b	Carbon precursor, flow rate (cm^3 min^{-1})	Additive, flow rate (cm^3 min^{-1})	Reaction temperature (°C)	Reaction time (min)	Support material	Properties of individual SWCNTs (if not otherwise specified)^d	References
NA	Co(NO$_3$)$_2$, (NH$_4$)$_6$Mo$_7$O$_{24}$	CO, 100		700	3–60	SiO$_2$ (gel)	Bundles $D \sim 1$ nm	[10, 46]
D_{ave} = 3.2, 9.0, 12.6	Fe(CO)$_5$	C$_2$H$_4$, 2–200 CH$_4$, 1000		800–1000	10	SiO$_2$ (oxidized Si)	$D_{CNT,ave} \sim$ 2.6, 7.3, 11.7 nm (DWCNTs, MWCNTs)	[5]
NA	Fe$_2$(SO$_4$)$_3$, (NH$_4$)$_6$Mo$_7$O$_{24}$	CH$_4$, 10–160	Ar, 430–280	680–850	60	Al$_2$O$_3$ (powder)	Individual and bundles $D = 0.8–1.5$ nm (Raman)	[47]
NA	Cobalt and iron salts^c	CH$_4$, 75	H$_2$, 300	1000	10	MgO (powder)	Individual and bundles $D = 0.8–5$ nm	[23]
NA	Cobalt, nickel and iron salts^c	C$_2$H$_4$, 30	N$_2$, 80	1080	60	Al$_2$O$_3$ (powder), SiO$_2$ (powder)	Individual and bundles $D = 0.7–5$ nm $L_B <$ several μm	[48]
NA	Co(NO$_3$)$_2$, Mg(NO$_3$)$_2$, Fe(NO$_3$)$_3$, Ni(NO$_3$)$_2$	CH$_4$, 45	H$_2$, 205	1000–1070	<6	MgO (from combustion) Mg$_{0.8}$Al$_2$O$_4$ (from combustion),	Individual and bundles $D = 0.5–5$ nm (DWCNTs, MWCNTs)	[21, 49]
NA	Fe(NO$_3$)$_3$	CH$_4$, 100		850	30	MgO Si (wafer)	Individual and bundles L up to several μm	[50]
<10, 20–30	Cobalt, molybdenum	CH$_4$, NA C$_2$H$_2$, NA		900	10–60	SiO$_2$ (oxidized Si)	(SWCNTs, DWCNTs)	[12, 51]
NA	FeCl$_2$ + Na$_2$MoO$_4$	CH$_4$, 800		900	15	Si (wafer), Si$_3$N$_4$ (membrane)	$D = 0.7–2.6$ nm	[17]
3–14, 2–3	Fe(CO)$_5$ + Mo(CO)$_6$, FeCl$_3$ + (NH$_4$)$_2$MoO$_4$	CH$_4$, 1200		900	30	SiH (wafer) SiO$_2$ (oxidized Si) Al$_2$O$_3$ (on Si)	NA $D = 0.9–2$ nm (AFM)	[11, 27]

Table 1. (Continued.)

Catalyst particle size (nm)[a]	Catalyst precursor compound[b]	Carbon precursor, flow rate (cm^3 min^{-1})	Additive, flow rate (cm^3 min^{-1})	Reaction temperature (°C)	Reaction time (min)	Support material	Properties of individual SWCNTs (if not otherwise specified)[d]	References
NA	$Fe(NO_3)_3$, $MoO_2(acac)_2$	CH_4, 1000–6000	H_2, 0–150	900–1000	7–10	Al_2O_3 (on Si wafer)	Individual and bundles $D \sim 1$–5 nm L_B up to over 10 μm	[52–54]
NA	Iron	CH_4, 600		600–800	5	Sapphire	Bundles $D \sim 1$–1.7 nm	[55]
NA	$FeCl_3$, MoO_2Cl_2	CH_4, 750–1000		900	20	SiO_2 and Al_2O_3 (on Si wafer)	Individual and bundles L up to 150 μm	[56, 57]
NA	Ferrocene	Benzene, 100–200	H_2, 300–500	1150	NA	NA	Individual and bundles $D = 1.1$–3 nm	[58]
<10	Fe_2O_3, iron, nickel	CH_4, 300		750–1000	1	SiO_2 (oxidized Si)	Bundles $D = 2$–3 nm (MWCNTs)	[59]

[a] Diameter measured before SWCNT growth.
[b] Water of hydration not included in the formula.
[c] Chemical composition not specified.
[d] From TEM image if not otherwise specified.

for both mechanisms has been presented by Cassell *et al* [9]. Furthermore, an alternative growth mechanism must be introduced to the CVD process. Evaporation of the catalyst metal may take place during CVD synthesis due to the physical properties of nanosized catalyst particles, as described in more detail later. The vaporized metal may nucleate and form secondary metal particles away from the surface. The catalytic decomposition reaction may then take place in the gas phase on the surface of the newly formed particles (as in aerosol synthesis). This product is eventually deposited on the reactor walls. Evidence of such a phenomenon has been observed during CVD when ruthenium has been used as a co-catalyst [9].

2.1. Catalyst particle properties

Nanosized transition metal particles, e.g. nickel, iron, molybdenum and cobalt, have been widely used in CVD either in oxide or metallic forms or as mixtures (refer to table 1). The most important property of the metals with regard to SWCNT formation is their ability to catalytically decompose gaseous carbon-containing molecules. Transition metals possess also other properties suitable for SWCNT synthesis, including melting temperature, equilibrium vapour pressure, solubility of carbon and carbon diffusion rate in the metal. Values of selected physico-chemical properties for several transition metals in the bulk form are listed in table 2. Note the similarities in the properties of the presented metals, with the exceptions of low carbon solubility in copper and high melting temperature and low equilibrium vapour pressure in molybdenum. All but copper are known catalysts for CNT production, implying that carbon solubility may be one of the most important properties of the catalysts.

2.1.1. Manufacturing methods. Several different manufacturing methods have been applied for the production of catalyst particles. The most common method is the precipitation of metal salts (nitrates, sulfates and chlorides), metal-organic or organometallic precursors on a support, followed by drying, calcining and grinding (see table 1 for references). After calcining, an oxide form of the catalyst material is obtained. The supported catalyst is then placed in the synthesis furnace, which is heated to the operating temperature typically in an inert argon or nitrogen atmosphere. Optionally, hydrogen flow is used to reduce the catalyst to metallic form during heating (e.g. [10, 11]).

Other, less common, methods for catalyst particle production for CVD include sputtering [12] and liquid chemistry routes such as the application of organic carriers [13–16]. Sputtering a metal target leads to the formation of a metal film on a support and subsequent heating transforms the film into metal particles. Organic carriers have been successfully utilized in the formation of uniformly sized catalyst particles as described later. An oxidation step is always necessary to remove the organic shell resulting in the formation of metal oxide particles. Subsequent introduction of hydrogen or hydrocarbon precursor results in metal oxide reduction, as described in more detail later.

2.1.2. Catalyst particle size. Several mechanistic studies have been conducted to determine the dependence of the CNT diameter on the catalyst particle size. Even in the first CVD publication by Dai *et al* [3] a close correlation between the SWCNT diameter and the connected catalyst particle was reported. Later, catalyst particles with predetermined size have been used to prove the connection [5, 13]. For instance, iron nanoparticles with average number mean diameters of 3, 9 and 13 nm, yielded CNTs with wall diameters of 3, 7 and 12 nm respectively as reported by Cheung *et al* [5]. The CNTs produced with the smallest catalyst particles were primarily SWCNTs with few double-walled carbon nanotubes (DWCNTs). With larger catalyst particles, the number of DWCNTs and thin MWCNTs increased in the product.

Table 2. Physico-chemical properties of selected transition metals. NA = data not available.

Macroscopic property	Iron	Cobalt	Nickel	Palladium	Copper	Molybdenum
Density, at 20 °C (liquid state) (kg m^{-3}) [60]	7874 (7035)	8900 (7670)	8902 (7780)	12020 (10379)	8960 (7940)	10220 (9330)
Melting temperature (T_{melt})(°C)	1536	1495	1453	1553	1083	2617
Surface tension at 20 °C (at 2000 °C) (N m^{-1}) [61]	1.95 (1.72)	2.1 (1.68)	1.86 (1.57)	2.1 (1.72)	1.75 (0.95)	2.2 (NA)
Equilibrium vapour pressure (at $t = 1216$ °C) (Pa) [62]	5.5×10^{-3}	4.7×10^{-3}	4.0×10^{-3}	2.1×10^{-2}	7.1×10^{-1}	7.6×10^{-11}
Carbon solubility (at.%) at T_{melt} [63]	20.2	13.9	10.7	$\sim$5	2×10^{-4}	Up to 60–70%
Carbon diffusion coefficient in metal (m^2 s^{-1}) (at $t = 1000$ °C) [64]	1.5×10^{-11}	1×10^{-11}	2×10^{-11}	6×10^{-11}	NA	NA

This finding has been the motivation for decreasing the catalyst particle size close to the 1–2 nm scale in order to produce the most desirable CNT product, i.e. SWCNTs.

Precipitation methods generally lead to wide particle size distributions. Therefore, several attempts have been made to control the size distribution and dispersion of catalyst particles. Organic carriers, such as apoferritin [13, 14] or polyamidoamine dendrimers [16], have been successfully used to decrease the spread of the nanoparticle size distribution to the 1–3 nm range. Similar results were also obtained with molybdenum oxide-based cage molecules [17]. Good dispersion of narrow size distribution particles on the support surface has been achieved with the use of dispersion agents such as acids and amines [5, 11, 18]. In all of the above-mentioned publications, the catalyst particle size was measured from transmission electron microscope (TEM) images before subjecting the catalyst to the SWCNT synthesis conditions.

Determining the particle size distribution before heating to the synthesis conditions gives only a rough estimate of catalyst particle size during the SWCNT nucleation and growth. Evolution of size distribution of the metal particles during the CNT synthesis is inevitable due to the increased temperature required to accelerate the decomposition of the carbon precursor molecules on the catalyst surface. When metal particles are heated, several different phenomena occur. Catalyst particles may collide due to surface diffusion. Subsequent sintering of particles has been observed to increase the average particle size (e.g. by Alvarez *et al* [10]). As a result of sintering, a reduced number concentration and increased mean size of catalyst particles is observed. Simultaneous evaporation of particles reduces the number concentration and modifies the size distribution even further, as acknowledged by Choi *et al* [16].

2.1.3. Chemical composition of the catalyst.   *In situ* measurements addressing the changes in chemical composition of the catalyst can elucidate the mechanisms taking place during CNT growth [10, 19]. The basic conclusion is that, when starting from an oxide catalyst, a reduction of metal oxide takes place during decomposition of the carbon precursor compound. As a result, a metallic particle forms through intermediate oxide states. Upon carbon dissolution, metal–carbon mixture or a metal carbide is formed. Subsequent segregation results in the formation of graphitic carbon and metal particles.

The yield of CNTs has been observed to increase with the use of bimetallic catalysts, e.g. cobalt–molybdenum [10], iron–molybdenum [20] and iron–cobalt [21]. Transition metals have different catalytic activities regarding carbon compound decomposition and carbon diffusion rates. Carbon compound decomposition on the surface of one metal and subsequent SWCNT growth from the other has been proposed [10]. *In situ* x-ray absorption spectroscopy (XANES and EXAFS) measurements of the cobalt–molybdenum catalyst show a reduction of cobalt oxide during SWCNT synthesis. Also a clear chemical transformation of molybdenum oxide to molybdenum carbide was observed. Several suggestions have been made regarding the role of the two metals in the synthesis. Molybdenum was thought to prevent sintering of the active cobalt oxide. Alternatively molybdenum carbide was described to work as a sink of carbon atoms thus controlling the feed rate of carbon to the active cobalt catalyst. However, the metals either separately or as a mixture of preformed single-metal particles did not selectively produce SWCNTs, suggesting that the bimetallic catalyst must be in the form of an alloy to present the highest activity. Further support comes from a study by Flahaut *et al* [21], in which *in situ* measurement of the chemical composition of an iron–cobalt catalyst shows that a transformation into an alloy takes place after reduction. The increase in catalytic activity of bimetallic catalysts can be understood on the basis of the physico-chemical properties of alloys. For instance, a decrease in melting temperature and an increase in carbon solubility are observed for alloys compared to single metals.

The use of metal oxide catalyst is regularly combined with hydrocarbons as the carbon precursor (refer to table 1). Decomposition of hydrocarbons releases hydrogen, which in turn reduces the oxide catalyst to metallic form. Also the released carbon takes part in the reduction reaction while dissolving in the catalyst particle, as described in more detail later. The timescale for the compositional changes of metal oxide catalysts during production of MWCNTs and carbon fibres via acetylene CVD on aluminium supported polycrystalline iron oxide film has been considered [19]. *In situ* x-ray photoelectron spectroscopy (XPS) and x-ray diffraction (XRD) show the steps of reduction and carbon dissolution. Reduction is observed when hydrogen is released from decomposing acetylene. MWCNT growth is observed approximately 20–30 min after the introduction of the hydrocarbon, when iron carbide starts to decompose to metallic iron and solid carbon. A similar timescale for SWCNT growth has been presented by Alvarez *et al* [10]. Only amorphous carbon is formed during the first 3 min. Longer reaction times are needed for abundant SWCNT growth. However, after 10 min growth slows down. The catalyst was present as an oxide during the fastest growth. The growth rate was reduced when conversion to metallic form took place. The active form of the catalyst metal is covered in more detail in the discussion.

2.2. Carbon precursor

In CVD synthesis of SWCNTs, the use of carbon precursor compounds has been, thus far, limited to methane (CH_4), acetylene (C_2H_2), ethylene (C_2H_4), carbon monoxide (CO), benzene and toluene (refer to table 1). Decomposition of the carbon precursors is discussed on the basis of thermodynamic calculations later. The feed rate of the carbon precursor compound to the catalyst particle surface is of key importance when the process is driven toward SWCNT formation. Increased temperatures are needed to accelerate the catalytic decomposition of hydrocarbon molecules and to increase the diffusion rate of carbon in the metal particle. However, increasing the temperature also increases the amount of self-pyrolysis of hydrocarbons. The most serious catalyst deactivation process in SWCNT synthesis is catalyst poisoning due to the accumulation of amorphous carbon. Accumulation of amorphous carbon may arise as a result of hydrocarbon self-pyrolysis or due to excessive carbon precursor concentration. Limiting the carbon precursor feed rate to the catalyst particle has been achieved by controlling the carbon precursor partial pressure (the case for hydrocarbons) and by selecting the carbon precursor according to the decomposition rate (CO disproportionates slowly at normal pressures) [5, 22]. The effect of the carbon precursor feed rate on the catalyst particle is clearly seen in Cheung *et al* [5], in which 9 nm catalyst particles were used to produce different products depending on the carbon precursor feed rate. With low carbon precursor concentration SWCNTs were produced, while increase in the available carbon led to the formation of thin MWCNTs. Furthermore, a linear variation in yield of SWCNTs according to partial pressure of the carbon precursor (ethylene) has been reported by Hafner *et al* [22].

2.3. Support–catalyst interaction

Several support materials have been used during CVD synthesis of SWCNTs. Most commonly aluminium oxide (Al_2O_3) and silicon dioxide (SiO_2) are used either in crystalline or amorphous form (see table 1). Other support materials include aluminium and oxidized silicon plates and silicon nitride membranes. Direct information regarding the growth mechanism of CNTs has been observed from samples in which the support consisted of a thin Al_2O_3 membrane deposited on a TEM grid [13]. Easy removal of support material from the SWCNT product has been reported with magnesium oxide as a support [23].

A prerequisite for a support material is thermal and chemical stability under the synthesis conditions [24]. Additional properties of proposed importance are the surface area and porosity of the support (e.g. [9]). Either chemical or physical interaction may take place between the support and the catalyst material. Physical interactions, e.g. van der Waals and electrostatic forces, together with obstruction of catalyst particle movement on the support surface due to surface roughness, reduce the thermally driven diffusion and sintering of metal particles on the support surface. This results in stabilization of the catalyst particle size distribution during SWCNT synthesis. Fumed aluminium oxide material consists of aluminium oxide nanocrystals and forms an anisotropic support surface making formation of catalyst particles with varying sizes and interaction types possible [25]. Fumed silicon dioxide, on the contrary, is an amorphous material and forms an isotropic support where catalyst particles may disperse more uniformly in the small pores. Consequently numerous SWCNTs grow in close proximity, resulting in bundle formation [13, 25]. A general feature of the CVD process is the reduction of SWCNT yield as a function of reaction time. Supports of higher porosity and surface area have been used to overcome this problem and, indeed, more linear growth rates have been reported [9, 26]. Introduction of high-porosity supports also leads to reduced sintering of catalyst particles as described above. Due to the lack of information about catalyst particle size during SWCNT growth, it is not yet possible to conclude whether the increased yield is a result of reduced sintering or more efficient diffusion of carbon precursor to the catalyst particles.

The chemical interactions between the catalyst particles and the surface groups of the support can also aid in maintaining the size distribution of the catalyst particles during SWCNT synthesis. If a strong chemical interaction takes place, particle growth is limited due to decreased particle mobility. 'Strong metal support interaction' (SMSI) may take place between easily reducible metal oxides and transition metals in the presence of hydrogen [24]. The most important SWCNT supports, however, are not easily reduced and the interaction via SMSI can be neglected. Aluminium oxide has been generally observed to be a superior support compared to silicon dioxide (e.g. [9, 25]). The stronger chemical interaction between aluminium oxide and metal particles has been appointed to either acidic [9] or basic [24] surface groups. Aluminium oxide is an amphoteric material presenting both acidic and basic sites, which may take part in chemical interactions. An increase in the electron density of the supported metal particles leads to stronger back donation of electrons from the catalyst particle to the carbon precursor compound, thus increasing the rate of carbon precursor decomposition [24].

Furthermore, interaction between the support lattice and the growing SWCNT has been reported by Su *et al* [27]. SWCNTs grown horizontally on silicon support surface with iron–molybdenum catalyst were observed to take preferred orientations depending on the lattice geometry of the support, so that on Si(100) two preferred orientations were found perpendicular to each other and on Si(111) three orientations with 60° angles were observed. The preferred orientations were attributed to maximum interaction between the SWCNT and the support. Also, in the case of native silicon oxide and overcoating with aluminium oxide, preservation of the preferred orientation according to the underlying silicon surface has been observed. Further experiments are needed to understand whether the lattice-oriented growth of SWCNTs is a result of SWCNT–support interactions or catalyst–support interactions, the latter giving rise to catalytic particles with variation in shape and size.

2.4. Reactor conditions and SWCNT growth rate

The experimental conditions (temperature, flow rate, reaction time) applied during CVD of SWCNTs are described in table 1. The reaction conditions have a profound effect on the

catalyst particle size evolution and on the rates of carbon precursor decomposition and carbon diffusion into the metal particles. A SWCNT growth rate of over 60 μm min^{-1} was reported by Kim *et al* [15]. However, information about the growth rate is generally absent from the literature. The weight gain of the SWCNTs during CVD decreases as the function of reaction time. The decrease has been attributed to physical obstruction in carbon precursor diffusion to the catalyst surface either by the growing mat of SWCNTs [9, 22], limited metal surface area due to the growing nanotube during the root-growth [14] or by accumulation of solid carbon. An alternative cause for the changes in catalytic activity could be the effect of catalyst particle size change during SWCNT growth, which should be considered in more detail in the future.

3. Aerosol synthesis of single-walled carbon nanotubes

Strictly speaking, the aerosol synthesis of SWCNTs should be performed entirely in the gas phase. The catalyst and carbon precursor vapours are continuously fed to a flow reactor with carrier gas, which can be either carbon precursor or additive gas. Subsequently, catalyst precursor decomposition and catalyst particle nucleation and growth followed by carbon precursor decomposition, carbon diffusion to the metal particle and precipitation in the form of SWCNT take place in the gas phase. The residence time in the reactor is in the range of seconds and it equals the time allowed for the above-mentioned processes to take place. The collection of the product is performed directly from the gas phase via aerosol particle collection methods (e.g. filters, cold collectors or electrostatic precipitators). In only in a few of the works dealing with gas-phase synthesis is the product collected directly from the gas phase [4, 6, 28]; the others combine aerosol synthesis and CVD methods and the term 'combined method' is used to distinguish these from the true aerosol synthesis experiments.

In combined methods, the SWCNT growth is performed in a flow reactor, the aerosol fed to the system consists of the catalyst and carbon precursor vapours and the reactions taking place in the system are analogous to those of aerosol synthesis. But this is where the similarities end. In the combined method, the residence time of the catalyst particle in the reactor can reach minutes or even hours. Both the metal clusters and the catalyst cluster containing SWCNTs formed in the gas phase may deposit to the reactor walls where the SWCNT growth may begin or continue via CVD. When the product is collected from the reactor walls after cooling, the determination of the growth method is very difficult. Also, during aerosol synthesis, SWCNT growth and deposition to the reactor walls followed by re-entrainment to the gas flow is possible. Thus, care should be taken in sample collection as well as in interpreting the results.

Table 3 summarizes the different experimental conditions applied in aerosol synthesis and the combined method of SWCNT production. Catalyst and carbon precursors, flow rates, reaction temperatures and times together with reactor tube dimensions and orientations are presented. Also the catalyst particle size after the SWCNT growth and the SWCNT product properties are listed as presented by the authors. Furthermore, catalyst precursor vapour pressures and flow Reynolds numbers have been calculated from the data given in the publications to clarify the conditions inside the reactor during the experiments. This section reviews results from aerosol synthesis as well as from combined method experiments.

3.1. Catalyst particle properties

3.1.1. Manufacturing methods.   Transition metals such as iron, cobalt, molybdenum and nickel are used as the catalyst material as in CVD. In aerosol synthesis and the combined method the catalyst particles are typically formed *in situ* via thermal decomposition of gaseous catalyst metal precursor molecules. Several different metal-containing compounds, such as

Table 3. Experimental conditions and product properties in aerosol synthesis and the combined method. NA = data not available, D_{ave} = average diameter, ID = inside diameter, OD = outside diameter, L = length, D = diameter, D_B = bundle diameter, L_B = bundle length.

Catalyst particle size (nm)	Catalyst precursor compound	Catalyst precursor vapour pressure (Pa)	Carbon precursor, flow rate (cm³ min⁻¹)	Additive, flow rate (cm³ min⁻¹)	Reactor tube dimensions (mm)	Reynolds number/ reactor orientation	Temperature (°C)/pressure (atm)	Reaction time	Product collection method	Properties of individual SWCNTs (if not otherwise specified)[c]	Refs.
NA	Fe(CO)$_5$	67	CO + H$_2$, 600–1200		ID = 20, L = 200	23.4–24.5/ horizontal	1000–1100/1	Few seconds	Cold collector, filter, from walls after cooling	Bundles D = 0.8–2.5 nm	[4]
$D_{ave} \sim 10.8$	CoCl$_2$, MoCl$_5$	11.5[a]	Benzene, Toluene	H$_2$, 1200	ID = 26, L = 1000	3.0/ vertical	1200/1	∼2.1s	Cold collector	Bundles D = 1.1–1.9 nm	[28]
$D_{ave} \sim 4$	Ni(acac)$_2$	∼5	CO, 330–420		ID = 22, L = 400	6.7–9.8/ vertical	923–1216/1	3–3.5 s	Electrostatic precipitation from gas phase	Individual D = 1–3 nm, L = 30–40 nm	[6]
NA	Ferrocene	346–444[a]	Benzene	H$_2$, 300	ID = 22, L = 600	6.1–6.5/ horizontal	1050–1180/1	NA	From walls after cooling	Bundles D_{ave} = 1 nm (Raman)	[32]
5–10	Fe(CO)$_5$	0–0.33	CO, 1000 −6000 + CH$_4$, 0–21		OD = 25.4 L = NA	6.7–104.6 horizontal	800–1200/ 1–10	NA	From walls after cooling, filter	D = 0.7–2.4 nm, $L_B \sim 1$ μm	[29]
NA	Cobaltocene, nickelocene, ferrocene, Fe(CO)$_5$	NA	C$_2$H$_2$, 50	Ar, 1000	ID = 10 L = NA	54.1/ horizontal	1100/1	NA	From walls after cooling	Individual and bundles D = 1–2 nm, L_B up to several μm (MWCNTs)	[33]
NA	Fe(CO)$_5$	0–50.6	CO, 9800		ID = 75 L = 1200	27705– 53481/ horizontal	900–1100/ 30–50	24–72 h	Filter, from walls after cooling	Bundles $D \sim 1$ nm	[30]
NA	Ferrocene	1.4–4.7[a]	C$_2$H$_2$, 3–10	Ar, 1200	ID = 30 L = NA	26.8–34.2/ horizontal	750–1200/1	NA	Cold collector, from walls after cooling	Individuals and bundles D_{ave} = 1.1 nm	[65]
NA	Ferrocene	0.04–0.6[a,b]	Benzene	H$_2$, 70–225 225	NA	NA/ horizontal	1100–1200/1	1–30 min	From walls after cooling	Bundles D = 1.0–4.3 nm, D_B = several nm–40 nm	[34, 66]

Table 3. (Continued.)

Catalyst particle size (nm)	Catalyst precursor compound	Catalyst precursor vapour pressure (Pa)	Carbon precursor, flow rate (cm^3 min^{-1})	Additive, flow rate (cm^3 min^{-1})	Reactor tube dimensions (mm)	Reynolds number/ reactor orientation	Temperature (°C)/pressure (atm)	Reaction time	Product collection method	Properties of individual SWCNTs (if not otherwise specified)[c]	Refs.
NA	Ferrocene	2703–4240[a]	n-hexane, benzene, 0.5–1	H$_2$, 100–250	ID = 58, L = 1600	0.9–1.4/ vertical	1050–1150/1	∼30 min	From walls after cooling	Bundles D = 1.1–2.1 nm (Raman), D_B = 10–70 nm (DWCNTs, MWCNTs)	[31, 67]

[a] Calculated from data given in publication.
[b] Vapour pressure calculated between vaporization temperature (185 °C) and decomposition temperature (400 °C) of ferrocene due to lack of a vaporization temperature.
[c] From TEM image if not otherwise specified.

chlorides, carbonyls, acetylacetonates or metallocenes, have been applied as the precursors (refer to table 3). Liquid precursors are introduced into the reactor as vapour, which is obtained by bubbling a carrier gas (which can be either the carbon precursor or an additive gas such as hydrogen, nitrogen or argon) through the liquid [4]. Alternatively injectors have been used to deliver liquid droplets directly to a hot reactor [29–31]. Solid precursors are heated to their vaporization temperature and the vapour is transported to the furnace with the carrier gas [32–34]. Furthermore, spraying of a solution consisting of previously made catalyst particles and solvent has been used to produce gas-phase catalyst particles [28]. However, sintering and evaporation in the reactor also changes the size distribution of the previously made metal particles and the particle size of the active catalysts may differ from those reported.

The formation of the metal catalyst particles via thermal decomposition of a metal-organic precursor has been described in detail by Nasibulin *et al* [6, 35]. Saturation of carrier gas with the metal precursor vapour was accomplished in a heated saturator, from which the precursor vapour (either copper or nickel acetylacetonate) was transported to the heated reactor. Thermal decomposition of the precursor molecules resulted in formation of supersaturated metal vapour in the reactor and, subsequently, to nucleation and metal particle growth via condensation, collision and sintering.

3.1.2. Catalyst particle size. The catalyst particle size has been investigated in aerosol synthesis even more rarely than in CVD (see table 3). Even though the particle size during CNT synthesis is typically not known, a few methods have been introduced to control the particle size to some extent. Rapid precursor decomposition has been achieved by using a water-cooled injector to feed the catalyst and carbon precursors directly into the hot reactor zone [29]. A further increase in the decomposition rate was achieved by mixing the room-temperature catalyst precursor in the hot reactor zone with preheated CO in turbulent jet flows [30]. Introduction of carbon precursor has been observed to passivate the metal particle surface and to consequently suppress the further growth of the metal particles [6]. Particle growth as a result of sintering may also be reduced by using diluted metal precursor concentrations. Furthermore, controlling the residence time in the reactor enables control over the catalyst particle size change.

3.2. Reactor conditions and SWCNT growth rate

To estimate the flow regime in the aerosol synthesis and combined method experiments, Reynolds numbers were calculated from the data given in the publications (see table 3). The Reynolds number is a dimensionless value describing the relative importance of inertial and viscous forces in a flow [36]. All but one experiment showed tube Reynolds numbers well below 2000, indicating a laminar flow. The tube Reynolds number in Bronikowski *et al* [30] implies a highly turbulent flow. Furthermore, a turbulent jet is applied to introduce the precursors into the reactor providing an additional source of turbulence. Also, Nikolaev *et al* [29] applied similar jets during precursor introduction causing turbulence in the flow, at least at the reactor inlet.

In a laminar flow reactor gradients of temperature and velocity are inevitably present. The parabolic velocity profile results in a distribution of particle residence times as a function of the radial distance from the tube axis [37]. Temperature gradient and residence time differences result in an ever-present distribution of particle sizes. The temperature and flow profiles of the SWCNT synthesis reactor have been discussed for the first time in detail by Nasibulin *et al* [6]. A fully developed laminar flow profile was predicted by computational fluid dynamics calculations. Furthermore, three different sections were identified in the reactor according to

temperature and reactions taking place as presented in figure 1. In the first section, called the initial zone, the temperature is increased from room temperature up to approximately 900 °C. In this section, the metal-organic precursor is decomposed and, subsequently, forms catalyst particles that initiate CO disproportionation. In the high-temperature zone, where the CO disproportionation reaction is prohibited, the only thermodynamically and kinetically likely process is carbon dissolution into the nickel particles. SWCNT precipitation is reported to occur upon cooling in the last section.

An association between the precipitation rate and the obtained product has been found [6]. Higher flow rate and consequently faster cooling and precipitation rates favour the formation of SWCNTs, while a slower precipitation rate yields encapsulated metal particles. During precipitation competition between two fluxes of carbon atoms takes place as presented schematically in figure 1. The segregation flux contributes to the flux of dissolved carbon atoms towards the particle surface. The diffusion flux accounts for diffusion of carbon atoms on the surface of the particles seeking their lowest energy states. If the precipitation rate is infinitely slow, an equilibrium structure will be achieved, i.e. the resulting form is layers of graphitic carbon surrounding a metal particle. However, due to the competition between segregation and diffusion fluxes, two situations can occur in the system depending on the precipitation rate. First, if the segregation flux is higher than the diffusion flux, initiation of SWCNT growth can occur, since there is insufficient time for the creation of the equilibrium structure. In this case, nucleation of SWCNTs is likely to occur from islands where the segregation flux is larger. Second, when the segregation flux is lower than the diffusion flux, carbon forms the thermodynamically most stable system—metal particles surrounded by graphitic layers.

A SWCNT production rate of 450 mg h^{-1} was reported by Bronikowski *et al* [30] in the combined method with an improved high-pressure CO disproportionation system. The SWCNT diameters in aerosol synthesis and the combined method are reported to range from 0.7 to 5 nm (refer to table 3). However, information regarding the length of individual SWCNTs is absent from the literature, with one exception: 30–40 nm long individual SWCNTs were generally produced via aerosol synthesis [6]. This result differs from the micron length SWCNT bundles reported in the combined method [29, 33]. The timescale of aerosol synthesis of SWCNTs is in the range of seconds. During this time catalyst precursor decomposition takes place followed by catalyst particle nucleation and growth via condensation, coalescence and sintering. Carbon precursor decomposition on the metal particle surface and carbon dissolution to metal followed by carbon precipitation must take place in order to produce SWCNTs. Due to the limited reaction time, a question arises as to whether carbon precursor decomposition followed by diffusion and precipitation of solid carbon are simultaneous processes or two subsequent steps. To address this question, a calculation was conducted on the maximum length of SWCNTs with diameters of 1 and 2.5 nm as a function of the diameter of metal particles with different carbon solubilities (figure 2). All of the carbon available for SWCNT growth was considered to be pre-dissolved. According to the calculation the maximum SWCNT length from the 1 to 5 nm catalyst particles is typically in the range of tens of nanometres. Increasing the solubility of carbon in metal and the metal particle diameter increase the SWCNT length. As an example, at 80 at.% solubility the carbon dissolved in a 4 nm metal particle yields an approximately 40 nm long SWCNT with a diameter of 2.5 nm, while the length of 1 nm diameter SWCNT reaches 100 nm under the same conditions. The result of the calculation coincides with the 30–40 nm SWCNT length observed in aerosol synthesis [6]. This could be evidence that carbon dissolution and segregation are in fact two consecutive steps. Due to the lack of length information in the other aerosol synthesis publications, the simultaneous or consecutive nature of SWCNT growth remains an open question. However, the formation of micron length SWCNT bundles or ropes entirely in the gas phase does not seem probable due
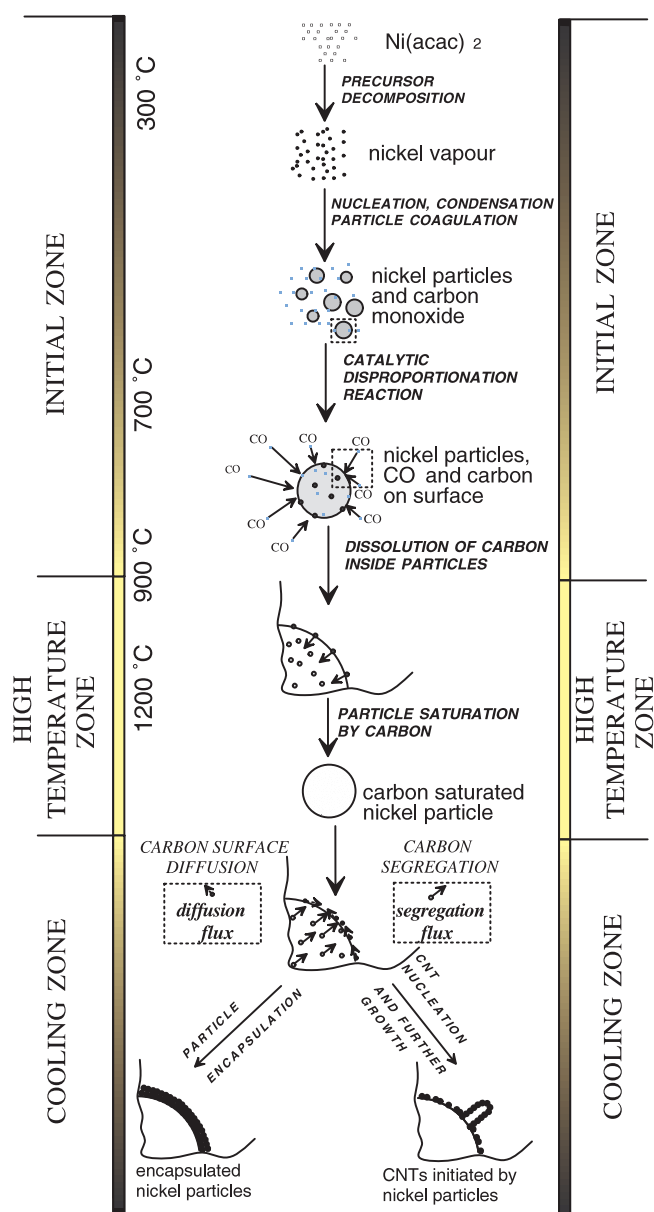
Figure 1. SWCNT formation mechanism during aerosol synthesis with nickel acetylacetonate as the catalyst precursor.

to the restricted residence time. The observed micron length SWCNT bundles are presumably a result of re-entrainment of SWCNT product from the reactor walls.

4. Discussion

4.1. Properties of nanoparticles

In chemical SWCNT production the diameter of the catalyst metal particles ranges from one to tens of nanometres. Decreasing the size of the metal particle to the nanometre scale results
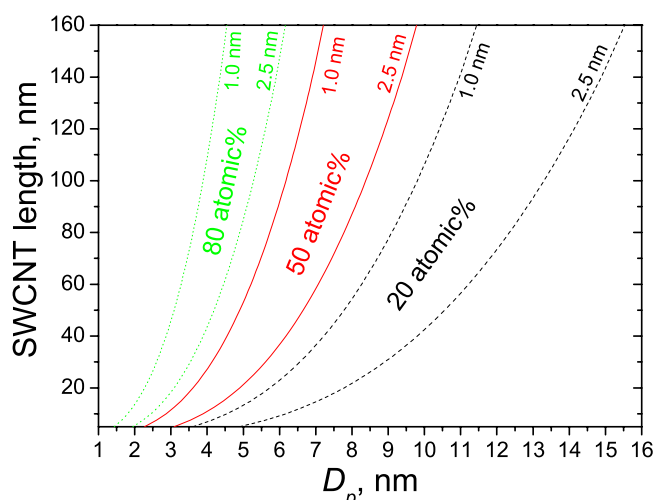
Figure 2. Length of 1 and 2.5 nm diameter SWCNTs with different carbon solubilities in metal as a function of catalyst particle diameter.

in a notable increase in the ratio of surface atoms to internal atoms. The atoms located on the surface are electronically and coordinatively unsaturated and, thus, are more reactive and mobile. This results in differences in various physical and chemical properties compared to the bulk material, e.g. lower melting temperatures and higher carbon solubilities in metals have been observed.

The melting temperature of metal particles smaller than approximately 100 nm can be lowered significantly [38]. The melting temperature of a particle (T_c) with a radius r can be approximated by

$$T_c = T_0 - \frac{2T_0}{\Delta H_{fusion}\rho_s r}\left[\sigma_{sl} + \left(1 - \frac{\rho_s}{\rho_l}\right)\sigma_l\right], \tag{1}$$

where T_0 is the bulk melting temperature, ΔH_{fusion} is the latent heat of fusion, ρ_s and ρ_l are the densities of solid and liquid metal respectively, σ_{sl} is the solid–liquid interfacial energy and σ_l is the surface energy of the liquid [39]. The melting temperature of iron, nickel, gold and silver as a function of particle diameter is presented in figure 3. The melting temperature is reduced from the bulk value for particles with diameters below 100 nm and a remarkable decrease is observed below 10 nm. On the basis of the presented calculation the 1–3 nm catalyst particles reported by several authors would, without any doubt, be in liquid form.

Equilibrium vapour pressures for bulk transition metals and carbon are presented in figure 4. Comparing the catalyst vapour pressures calculated for the aerosol synthesis and combined method experiments (table 3) with the bulk metal equilibrium vapour pressures, we observe that the vapour pressures in the experiments exceed the equilibrium vapour pressures of the metals. This indicates that a supersaturation condition is achieved in the reactor, enabling nucleation and growth of catalyst particles via condensation and coagulation. However, the high curvature of nanoparticle surface modifies the equilibrium vapour pressure. This can be approximated by

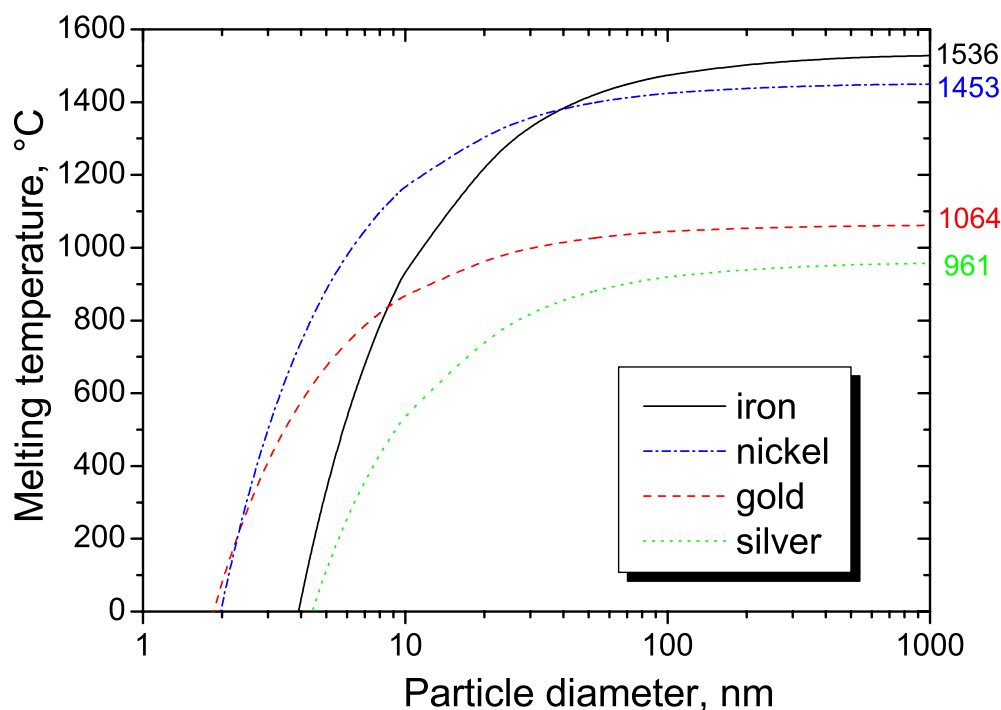$$p = p_0 \exp\left(\frac{2\sigma V}{kTr}\right), \tag{2}$$

Figure 3. Melting temperature of selected metals as a function of particle diameter.

where p and p_0 are the vapour pressures over curved and flat surfaces, respectively [36]. σ is the surface tension and V is the volume of a metal molecule. Simply stated the curvature of the nanoparticle surface results in fewer interacting neighbouring atoms and consequently in smaller attractive forces between the atoms providing for easier escape of atoms from the surface. The equilibrium vapour pressure over a curved surface as a function of metal particle diameter according to equation (2) is presented in figure 5 for iron and nickel at their melting temperatures. The increase in the equilibrium vapour pressure of catalyst particles in the 1–5 nm size range is noteworthy. This so-called Kelvin effect can lead to evolution of the catalyst particle size distribution due to evaporation of catalyst particles during CNT nucleation and growth.

The solubility of carbon in metal is a temperature-dependent property, which increases with increasing temperature. The solubility of carbon in transition metals can be significantly increased due to the small size of the catalyst particles. The effect of particle size on the solubility of carbon in metal particles is analogous to the vapour pressure and can be estimated as

$$S = S_0 \exp\left(\frac{2\sigma V}{kTr}\right), \tag{3}$$

where S and S_0 are solubilities in the particle and bulk material respectively, defined as the ratio of the amounts of solute and solvent [40]. The size-dependent solubilities of carbon in nickel and iron at the metal melting temperatures are presented in figure 6, where the solubility is presented as the atomic percentage. The bulk solubility of carbon in nickel is 10.7 and in iron 20.2 at.%. The solubility of carbon in iron and nickel increases for metal particles with a diameter of less than approximately 10 nm. For 1 nm diameter iron and nickel particles
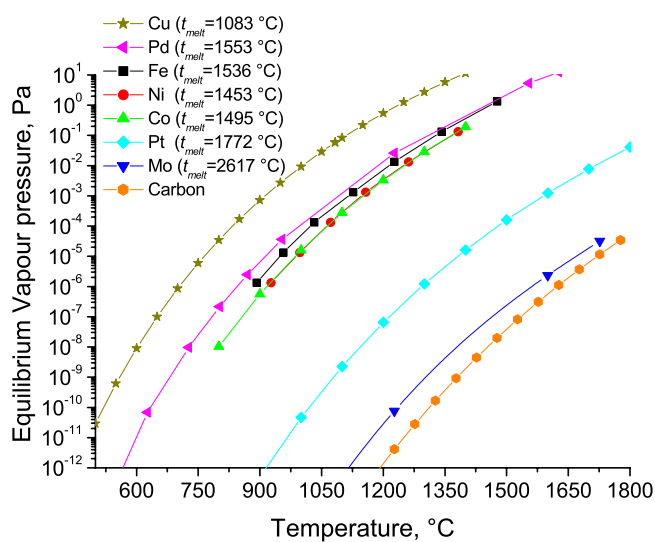
Figure 4. Equilibrium vapour pressure of selected metals and carbon as a function of temperature.
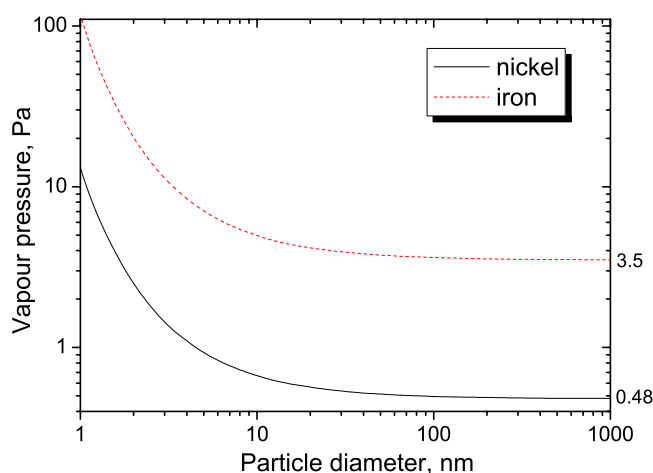

Figure 5. Equilibrium vapour pressure of iron and nickel at the metal melting temperature as a function of particle diameter.

over 80% carbon solubility is observed, which implies that more than 4 mol of carbon can be dissolved in 1 mol of iron.

According to the experimental data, the use of metal oxide catalysts has been limited to conditions where reduction of metal oxide is possible (see table 1). Either hydrocarbon precursors, which upon decomposition release hydrogen and carbon, or reduction by hydrogen before addition of carbon precursor are used. The simultaneously present dissolved carbon and oxygen react and form dissolved CO in the liquid metal particle ($\{C\} + \{O\} = \{CO\}$). Due to the fact that thermodynamic data for iron are readily available, we demonstrate this by calculating the equilibrium constant for the above-mentioned reaction in liquid iron particles
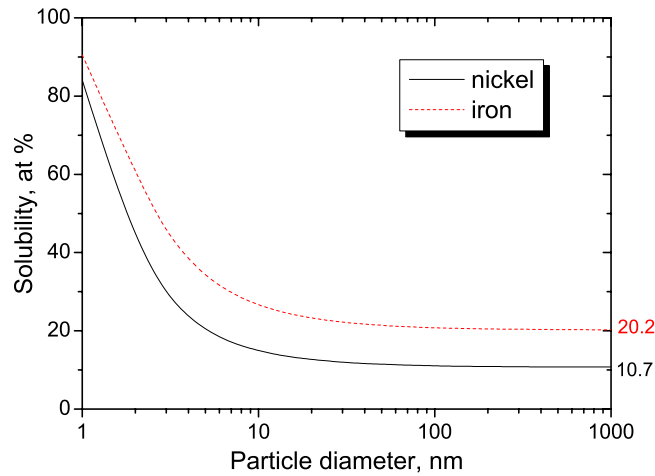
Figure 6. Solubility of carbon in iron and nickel at the metal melting temperature as a function of particle diameter.

according to

$$K = \frac{P_{CO}}{[C][O]f_C f_O} = 10^{1160/T+2.00}, \tag{4}$$

where [C] and [O] are the equilibrium concentrations of carbon and oxygen respectively in at.% in the metal [41]. The activity coefficients f_C and f_O can be found on the basis of interaction parameters e_O of oxygen in the presence of oxygen and carbon (e_O^O and e_O^C respectively) and of carbon e_C in the presence of oxygen and carbon (e_C^O and e_C^C respectively) as

$$\lg f_O = e_O^O[O] + e_O^C[C] \tag{5}$$

and

$$\lg f_C = e_C^C[C] + e_C^O[O], \tag{6}$$

where $e_O^O = -1750/T + 0.734$, $e_O^C = -0.41$, $e_C^C = 158/T + 0.0581$ and $e_C^O = -0.34$ [41]. Figure 7 presents the equilibrium concentrations of dissolved carbon and oxygen in liquid iron particles at two different CO partial pressures. Even at a CO partial pressure of 1 atm the equilibrium concentration of dissolved oxygen in iron is very low (below 0.01 at.%) given that about 1 at.% dissolved carbon is present. Increasing the concentration of either carbon or oxygen results in further release of CO from the particle. At lower CO partial pressures the effect is even more pronounced. This result provides further proof that metal oxides cannot act as catalyst particles for SWCNT growth and that the active catalyst exists in the form of reduced metal. Note that the result does not imply that a metal oxide particle is unable to catalyse the carbon precursor decomposition reaction. Only dissolution of carbon atoms and precipitation of solid carbon from metal oxide catalyst particles is impossible due to the formation of CO.

4.2. Thermodynamics and kinetics of carbon precursor decomposition

Hydrocarbon molecules decompose at high temperatures even without the presence of catalysts. Thermodynamic calculations performed using the FactSage database [42] on the stability of gaseous and liquid hydrocarbon molecules are presented as Gibb's free energy change
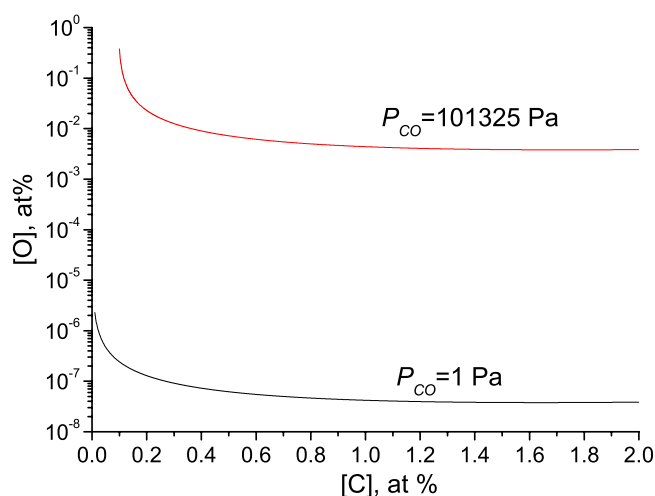
Figure 7. Equilibrium concentrations of carbon and oxygen in liquid iron.

of the decomposition reaction in figure 8. Increasing the number of carbon atoms in saturated hydrocarbons (CH_4, C_2H_6 and C_3H_8) leads to a decrease in the stability of the molecules. Methane is the most stable hydrocarbon and its thermal decomposition begins at approximately 900 °C [43]. Unsaturated hydrocarbons (C_2H_2 and C_2H_4) have more easily disrupted π-bonds in their structure and are thus more reactive and unstable. According to the thermodynamic calculations, the decomposition of unsaturated hydrocarbons (by the reaction $C_xH_y \rightarrow xC + 1/2yH_2$) is already favourable at the lowest calculated temperature (200 °C). As an example, acetylene is thermodynamically unstable already at 25 °C and decomposes to numerous products (including CH_4 and C_2H_4) according to complex kinetics [44]. However, the decomposition reaction is not self-sustaining and it stops without additional energy or the presence of oxygen. At high temperatures the decomposition proceeds readily and the reaction products may undergo further reactions, such as decomposition and polymerization. Due to this complex self-pyrolysis, the concentration of hydrocarbons must be controlled in order to prevent catalyst deactivation by amorphous carbon accumulation. The use of liquid hydrocarbon precursors has been limited to benzene and toluene, which can be easily understood by the results of the thermodynamic calculations. As with saturated hydrocarbons, the stability of the aromatic precursor molecules (benzene, toluene, o-xylene and 1, 2, 4-trimethylbenzene) decreases with an increasing number of methyl groups.

Carbon monoxide has a simple disproportionation reaction, making it an ideal carbon precursor for SWCNT synthesis:

$$2CO\ (g) \leftrightarrow CO_2\ (g) + C\ (s), \qquad \Delta H = -171 \text{ kJ mol}^{-1}. \qquad (7)$$

However, the reaction is exothermic and proceeds toward the initial products at high temperatures. Thermodynamic data on the disproportionation reaction are shown in detail in figure 9. The temperature dependence of equilibrium mole fraction of CO at different pressures together with results from kinetic investigations of CO disproportionation at the surface of high-porosity nickel [45] are presented. As a conclusion, kinetic and thermodynamic factors limit the effective CO disproportionation reaction to a temperature range of 520–800 °C at normal pressure. This temperature range may not be optimal for carbon dissolution and precipitation from the metal particle. Increasing the CO pressure shifts the effective CO disproportionation reaction temperature range to higher temperatures, as shown in figure 9. Increasing the pressure
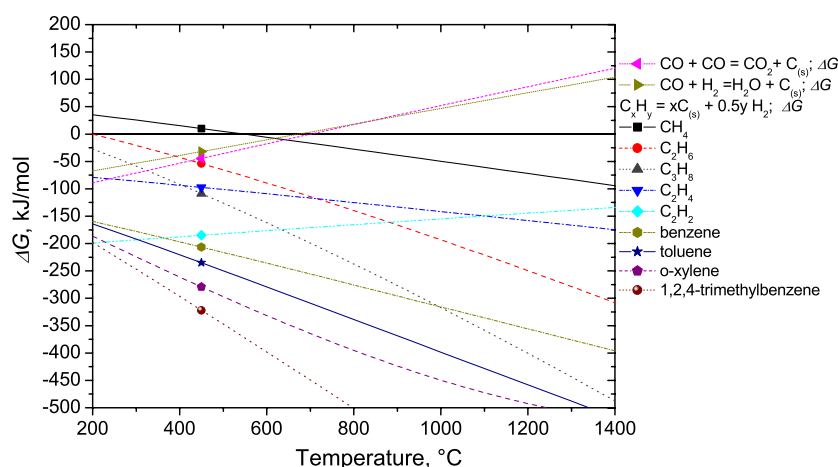
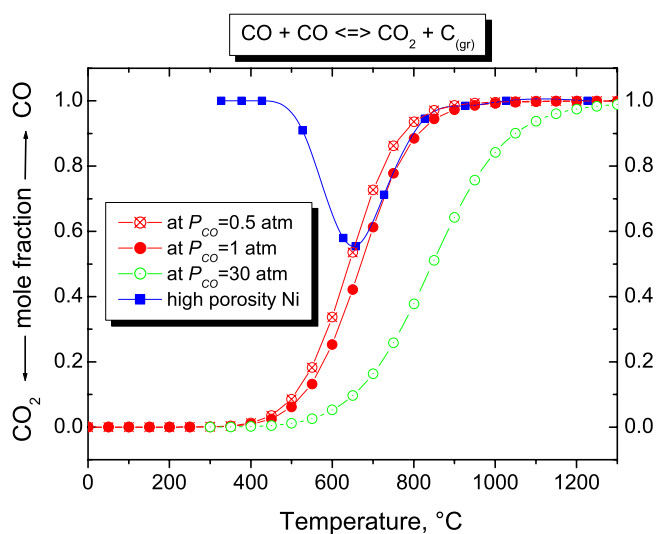**Figure 8.** Thermodynamic data for hydrocarbon and carbon monoxide decomposition.

Figure 9. Equilibrium concentration of CO at different pressures and kinetic data for CO disproportionation on the surface of high-porosity nickel as a function of temperature.

has been observed to increase the SWCNT production rate as well as to favour the production of SWCNTs with smaller average diameter [29].

Addition of hydrogen (H_2) has been reported to increase the yield of SWCNTs [4]. The increase was credited to hydrogenation of CO according to the reaction:

$$CO \text{ (g)} + H_2 \text{ (g)} \leftrightarrow H_2O \text{ (g)} + C \text{ (s)}, \qquad \Delta H = -135 \text{ kJ mol}^{-1}. \qquad (8)$$
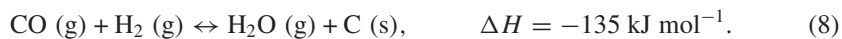
However, during high-pressure CO disproportionation addition of hydrogen was observed to either decelerate the reaction or to be ineffective [30]. According to thermodynamic calculations, addition of hydrogen does not notably affect the decomposition of CO (see figure 8).

4.3. Future work

Due to their unique properties, the SWCNTs have attracted worldwide attention among researchers. Several applications have already been suggested and demonstrated for this extraordinary material. However, more uses are likely to be proposed in the future. Currently chemical methods are developed toward substantial production of SWCNTs. In particular aerosol synthesis of SWCNTs has great potential for large-scale production of this desired product due to its continuous nature. However, in the future, the selective production of small quantities of SWCNTs with appropriate properties may become more desirable than abundant production of SWCNTs with a distribution of properties. In principal, the production of even one SWCNT with appropriate properties at the right time and in the right place may be enough for a specific application. For this purpose the understanding of the SWCNT growth mechanism is essential. However, to date a mechanistic understanding of SWCNT formation is lacking. Combined modelling of fluid flow and the aerosol dynamics, i.e. catalyst particle formation and size evolution, carbon precursor decomposition and carbon precipitation, is needed to understand and control the interconnected phenomena. Information regarding the catalyst particle size and SWCNT diameter distributions as well as their transformations in the flow reactor is rarely found in the literature, while the SWCNT length distributions are mostly ignored. However, these distributions could provide valuable information regarding the evolution of catalyst particle size and the SWCNT growth mechanism, especially in aerosol synthesis.

Methods to produce truly monodisperse catalyst particle size distributions and the ability to control the changes in the size distribution are required for better control of SWCNT properties and for more efficient catalyst utilization. Nucleating agents to help produce smaller particles combined with separation of nucleation and growth zones in multiple-temperature-zone reactors have been suggested [30].

5. Conclusions

Chemical SWCNT formation includes steps of catalyst particle formation, carbon precursor decomposition via catalytic reaction at the catalyst surface, dissolution of carbon atoms into the catalyst particle and solid carbon precipitation due to carbon supersaturation in the catalyst particle. The form of the precipitated carbon is dictated by the catalyst particle size, carbon feed rate and reactor conditions. Also the carbon precipitation rate affects the form of precipitated carbon in aerosol synthesis. The active catalyst metal in SWCNT synthesis is in reduced form according to experimental data and calculations regarding the equilibrium concentration of carbon and oxygen in iron. Activation of metal oxide particles thus requires a time-consuming reduction step. Correlation between the catalyst particle size and SWCNT diameter has been the motivation to reduce the catalyst particle size down to 1–3 nm. Evolution of the catalyst particle size distribution during SWCNT synthesis is inevitable due to collision and evaporation of metal particles at high temperatures. In CVD the physical and chemical interactions between catalyst particle and support surface groups may be utilized in controlling the evolution of the particle size distribution. In aerosol synthesis the velocity and temperature gradients in the flow reactor result in a distribution of particle sizes.

Physico-chemical properties of nanoparticles differ from the bulk values due to the high ratio of surface atoms to internal atoms. Significant changes in the metal melting temperature can be observed for particles below 100 nm. The 1–3 nm catalyst particles are preferably in liquid form during growth of SWCNTs. Evaporation of nanoparticles during SWCNT formation is possible due to the Kelvin effect. The solubility of carbon in transition metals

is increased significantly as the particle size is reduced. In CVD the reaction time can reach hours and carbon dissolution and precipitation may occur simultaneously. However, in the aerosol synthesis of SWCNTs, the residence time is in the range of seconds. The calculation regarding the maximum length of 1 and 2.5 nm diameter SWCNTs as a function of catalyst particle size shows that lengths of the order of tens of nanometres are obtainable from pre-dissolved carbon. Comparing this result with the observed SWCNT lengths suggests that in the aerosol synthesis method carbon dissolution and precipitation may be consecutive rather than simultaneous steps.

The feed rate of carbon to the metal particles must be controlled in order to selectively produce SWCNTs and to avoid accumulation of amorphous carbon. Thermodynamic calculations on the decomposition of hydrocarbon molecules show that increasing the number of carbon atoms in saturated hydrocarbons results in a decrease of molecule stability and consequently to self-pyrolysis at lower temperatures. Unsaturated hydrocarbons are more reactive due to π-bonding. Increasing the number of methyl groups in aromatic hydrocarbons increases the instability of the molecule. Thermodynamic and kinetic investigations on CO disproportionation show appropriate reaction rates only at 520–800 °C. Increased pressure may be applied to increase the reaction rate at higher temperatures.

Acknowledgments

References

[1] Iijima S 1991 *Nature* **354** 56–8
[2] Guo T, Nikolaev P, Thess A, Colbert D T and Smalley R E 1995 *Chem. Phys. Lett.* **243** 49–54
[3] Dai H, Rinzler A G, Nikolaev P, Thess A, Colbert D T and Smalley R E 1996 *Chem. Phys. Lett.* **260** 471–5
[4] Bladh K, Falk L K L and Rohmund F 2000 *Appl. Phys.* A **70** 317–22
[5] Cheung C L, Kurtz A, Park H and Lieber C M 2002 *J. Phys. Chem.* B **106** 2429–33
[6] Nasibulin A G, Moisala A, Brown D P and Kauppinen E I 2003 *Carbon* at press
[7] Dai H 2002 *Surf. Sci.* **500** 218–41
[8] Dresselhaus M S, Dresselhaus G and Eklund P C 1996 *Science of Fullerenes and Carbon Nanotubes* (San Diego, CA: Academic) p 965
[9] Cassell A M, Raymakers J A, Kong J and Dai H 1999 *J. Phys. Chem.* B **103** 6484–92
[10] Alvarez W E, Kitiyanan B, Borgna A and Resasco D E 2001 *Carbon* **39** 547–58
[11] Li Y, Liu J, Wang Y and Wang Z L 2001 *Chem. Mater.* **13** 1008–14
[12] Yoon Y J, Bae J C, Baik H K, Cho S J, Lee S-J, Song K M and Myung N S 2002 *Physica* B **323** 318–20
[13] Li Y, Kim W, Zhang Y, Rolandi M, Wang D and Dai H 2001 *J. Phys. Chem.* B **105** 11424–31
[14] Zhang Y, Li Y, Kim W, Wang D and Dai H 2002 *Appl. Phys.* A **74** 325–8
[15] Kim W, Choi H C, Shim M, Li Y, Wang D and Dai H 2002 *Nano Lett.* **2** 703–8
[16] Choi H C, Kim W, Wang D and Dai H 2002 *J. Phys. Chem.* B **106** 12361–5
[17] An L, Owens J M, McNeil L E and Liu J 2002 *J. Am. Chem. Soc.* **124** 13688–9
[18] Choi H C, Kundaria S, Wang D, Javey A, Wang Q, Rolandi M and Dai H 2003 *Nano Lett.* **3** 157–61
[19] Emmenegger C, Bonard J-M, Mauron P, Sudan P, Lepora A, Grobety B, Züttel A and Schlapbach L 2003 *Carbon* **41** 539–47
[20] Harutyunyan A R, Pradhan B K, Kim U J, Chen G and Eklund P E 2002 *Nano Lett.* **2** 525–30
[21] Flahaut E, Govindaraj A, Peigney A, Laurent Ch, Rousset A and Rao C N R 1999 *Chem. Phys. Lett.* **300** 236–42
[22] Hafner J H, Bronikowski M J, Azamian B R, Nikolaev P, Rinzler A G, Colbert D T, Smith K A and Smalley R E 1998 *Chem. Phys. Lett.* **296** 195–202

[23] Colomer J-F, Stephan C, Lefrant S, Van Tendeloo G, Willems I, Kónya Z, Fonseca A, Laurent Ch and Nagy J B 2000 *Chem. Phys. Lett.* **317** 83–9
[24] van der Wal R L, Ticich T M and Curtis V E 2001 *Carbon* **39** 2277–89
[25] Kong J, Cassell A M and Dai H 1998 *Chem. Phys. Lett.* **292** 567–74
[26] Su M, Zheng B and Liu J 2000 *Chem. Phys. Lett.* **322** 321–6
[27] Su M, Li Y, Maynor B, Buldum A, Lu J P and Liu J 2000 *J. Phys. Chem.* B **104** 6505–8
[28] Ago H, Ohshima S, Uchida K and Yumura M 2001 *J. Phys. Chem.* **105** 10453–6
[29] Nikolaev P, Bronikowski M J, Bradley R K, Rohmund F, Colbert D T, Smith K A and Smalley R E 1999 *Chem. Phys. Lett.* **313** 91–7
[30] Bronikowski M J, Willis P A, Colbert D T, Smith K A and Smalley R E 2001 *J. Vac. Sci. Technol.* A **19** 1800–5
[31] Zhu H, Li X, Xu C and Wu D 2002 *Mater. Res. Bull.* **37** 177–83
[32] Ci L, Wei J, Wei B, Liang J, Xu C and Wu D 2001 *Carbon* **39** 329–35
[33] Satishkumar B C, Govindaraj A, Sen R and Rao C N R 1998 *Chem. Phys. Lett.* **293** 47–52
[34] Cheng H M, Li F, Su G, Pan H Y, He L L, Sun X and Dresselhaus M S 1998 *Appl. Phys. Lett.* **72** 3282–4
[35] Nasibulin A G, Altman I S and Kauppinen E I 2003 *Chem. Phys. Lett.* **367** 771–7
[36] Hinds W C 1998 *Aerosol Technology: Properties, Behaviour, and Measurement of Airborne Particles* 2nd edn (New York: Wiley–Interscience) p 483
[37] Schliching H 1975 *Boundary Layer Theory* 7th edn (New York: McGraw-Hill) p 817
[38] Buffat Ph and Borel J-P 1976 *Phys. Rev.* A **13** 2287–98
[39] Friedlander S K 2000 *Smoke, Dust, and Haze* 2nd edn (New York: Oxford University Press) p 407
[40] Hochella M F Jr 2002 *Geochim. Cosmochim. Acta* **66** 735–43
[41] Arsent'ev P P, Paderin S N, Serov G V, Ryzhonkov D I, Krasheninnikov M G and Kazakov N B 1989 *Eksperimental'nye Raboty Po Teorii Metallurgocheskih Protcessov (Experimental Works on Theory of Metallurgical Processes)* (Moscow: Metallurgija) p 288
[42] Bale C W, Chartrand P, Degterov S A, Eriksson G, Hack K, Mahfoud R B, Melançon J, Pelton A D and Petersen S 2002 *Calphad* **26** 189–228
[43] Shah N, Panjala D and Huffman G P 2001 *North American Catalysis Society Mtg, (Toronto, Canada, June 2001)*
[44] Pässler P, Hefner W and Wernicke H-J 1985 *Ullmann's Encyclopedia of Industrial Chemistry* vol A1 (Weinheim: VCH) pp 97–145
[45] Panjushin L A and Smirnov Yu P 1988 *Laboratornyi Praktikum Po Teorii Metallurgicheskih Protcessov (Laboratory Practical Works on Theory of Metallurgy Processes)* (Leningrad: Leningradskii Politekhnicheskii Institut) p 88
[46] Kitiyanan B, Alvarez W E, Harwell J H and Resasco D E 2000 *Chem. Phys. Lett.* **317** 497–503
[47] Hornyak G L, Grigorian L, Dillon A C, Parilla A, Jones K M and Heben M J 2002 *J. Phys. Chem.* B **106** 2821–5
[48] Colomer J-F, Bister G, Willems I, Kónya Z, Fonseca A, Van Tendeloo G and Nagy J B 1999 *Chem. Commun.* 1343–4
[49] Flahaut E, Peigney A, Laurent Ch and Rousset A 2000 *J. Mater. Chem.* **10** 249–52
[50] Yan H, Li Q, Zhang J and Liu Z 2002 *Carbon* **40** 2693–8
[51] Yoon Y J, Bae J C, Baik H K, Cho S J, Lee S-J, Song K M and Myung N S 2002 *Chem. Phys. Lett.* **366** 109–14
[52] Kong J, Soh H T, Cassell A M, Quate C F and Dai H 1998 *Nature* **395** 878–81
[53] Franklin N R, Li Y, Chen R J, Javey A and Dai H 2001 *Appl. Phys. Lett.* **79** 4571–3
[54] Soh H T, Quate C F, Morpurgo A F, Marcus C M, Kong J and Dai H 1999 *Appl. Phys. Lett.* **75** 627–9
[55] Hongo H, Yudasaka M, Ichihashi T, Nihey F and Iijima S 2002 *Chem. Phys. Lett.* **361** 349–54
[56] Cassell A M, Franklin N R, Tombler T W, Chan E M, Han J and Dai H 1999 *J. Am. Chem. Soc.* **121** 7975–6
[57] Franklin N R and Dai H 2000 *Adv. Mater.* **12** 890–4
[58] Yang Q H, Bai S, Fournier T, Li F, Wang G, Cheng H M and Bai J B 2003 *Chem. Phys. Lett.* **370** 274–9
[59] Homma Y, Yamashita T, Finnie P, Tomita M and Ogino T 2002 *Japan. J. Appl. Phys.* **41** L89–91
[60] Emsley J 1991 *The Elements* (Oxford: Clarendon) p 264
[61] German R M 1996 *Sintering Theory and Practice* (New York: Wiley–Interscience) p 550
[62] Kulikov I S 1986 *Termodinamika Oksidov (Thermodynamics of Oxides)* (Moscow: Metallurgija) p 344
[63] Kulikov I S 1988 *Termodinamika Karbidov i Nitridov (Thermodynamics of Carbides and Nitrides)* (Chelybinsk: Metallurgija) pp 149–52
[64] Yokoyama H, Numakura H and Koiwa M 1998 *Acta Mater.* **46** 2823–30
[65] Ci L, Xie S, Tang D, Yan X, Li Y, Liu Z, Zou X, Zhou W and Wang G 2001 *Chem. Phys. Lett.* **349** 191–5
[66] Cheng H M, Li F, Sun X, Brown S D M, Pimenta M A, Marucci A, Dresselhaus G and Dresselhaus M S 1998 *Chem. Phys. Lett.* **289** 602–10
[67] Zhu H W, Xu C L, Wu D H, Wei B Q, Vajtai R and Ajayan P M 2002 *Science* **296** 884–6